SHRIMP ZIRCON AGES AND PETROLOGY OF LOWER CRUSTAL GRANULITE XENOLITHS FROM THE LETSENG-LA-TERAE KIMBERLITE, LESOTHO: FURTHER EVIDENCE FOR A NAMAQUA-NATAL CONNECTION

H. SOMMER
Corresponding author: School of Geography, Earth Science and Environment, The University of the South Pacific, Laucala Campus, Suva, Fiji Islands
e-mail: info@holgersommer.de

Y. WAN
Institute of Geology and Beijing SHRIMP Centre, Chinese Academy of Geological Sciences, 26 Baiwanzhuang Road, Beijing 100037, China
e-mail: wanyusheng@bjshrimp.cn

A. KRÖNER
Institute of Geology and Beijing SHRIMP Centre, Chinese Academy of Geological Sciences, 26 Baiwanzhuang Road, Beijing 100037, China
Institut für Geowissenschaften, Universität Mainz, D-55099 Mainz, Germany
e-mail: kroener@uni-mainz.de

H. XIE
Institute of Geology and Beijing SHRIMP Centre, Chinese Academy of Geological Sciences, 26 Baiwanzhuang Road, Beijing 100037, China
email: rock@bjshrimp.cn

D.E. JACOB
Department of Earth and Planetary Science, Macquarie University, North Ryde, NSW 2109, Australia
e-mail: dorrit.jacob@mq.edu.au

ABSTRACT

Recrystallized zircons extracted from intermediate granulites of the Letseng-la-Terae Diamond Mine in northeastern Lesotho provide evidence that the Tugela Terrane of the Mesoproterozoic high-grade Namaqua-Natal mobile belt may extend ~200 km farther west than previously thought. The rock-forming minerals in the investigated lower crustal granulites contain garnet, clinopyroxene, plagioclase and quartz or garnet, wollastonite, plagioclase and quartz. Calculated values for peak granulite-facies metamorphism are ~13 kbar and ~850°C. Thermal overprint and therein granulite-facies metamorphism occurred during the late Mesoproterozoic and is documented by SHRIMP metamorphic zircon ages of 1018 ± 18, 1126 ± 10 and 1127 ± 6 Ma. These ages are in good agreement with the timing of other events in the Namaqua-Natal belt. High-grade metamorphism was probably caused by crustal thickening resulting from continent-arc collision, followed by underplating of hot mantle melts.

Introduction

The origin, age and composition of lower crustal granulites are key issues to understand the complex interactions between geodynamic processes during subduction, collision and continental growth. Two models generally explain high-temperature granulite-facies metamorphism: The first model necessitates a high geothermal gradient to add heat from convective mantle through melt flux (De Yoreo et al., 1991; Vanderhaeghe and Duchene, 2010; Vanderhaeghe, 2012). The emplacement of dense mafic melts beneath more buoyant crust is named "magmatic underplating" (Drummond and Collins, 1986; Lodge et al., 2012; Zartman et al., 2012). Several Proterozoic and Phanerozoic crustal domains are characterized by seismically fast lower crust that probably formed through such magmatic underplating (Drummond and Collins, 1986; Durrheim and Mooney, 1994; Lodge et al., 2012; Zartman et al., 2012). The second model is related to crustal thickening caused by collisional orogeny or terrane accretion. This creates high thermal gradients in the lower crust due to thickening of a layer with relatively high radiogenic heat production and upward advection of heat during erosional isostatic re-equilibration (England and Thompson, 1984a; b).

doi:10.2113/gssajg.116.2.183

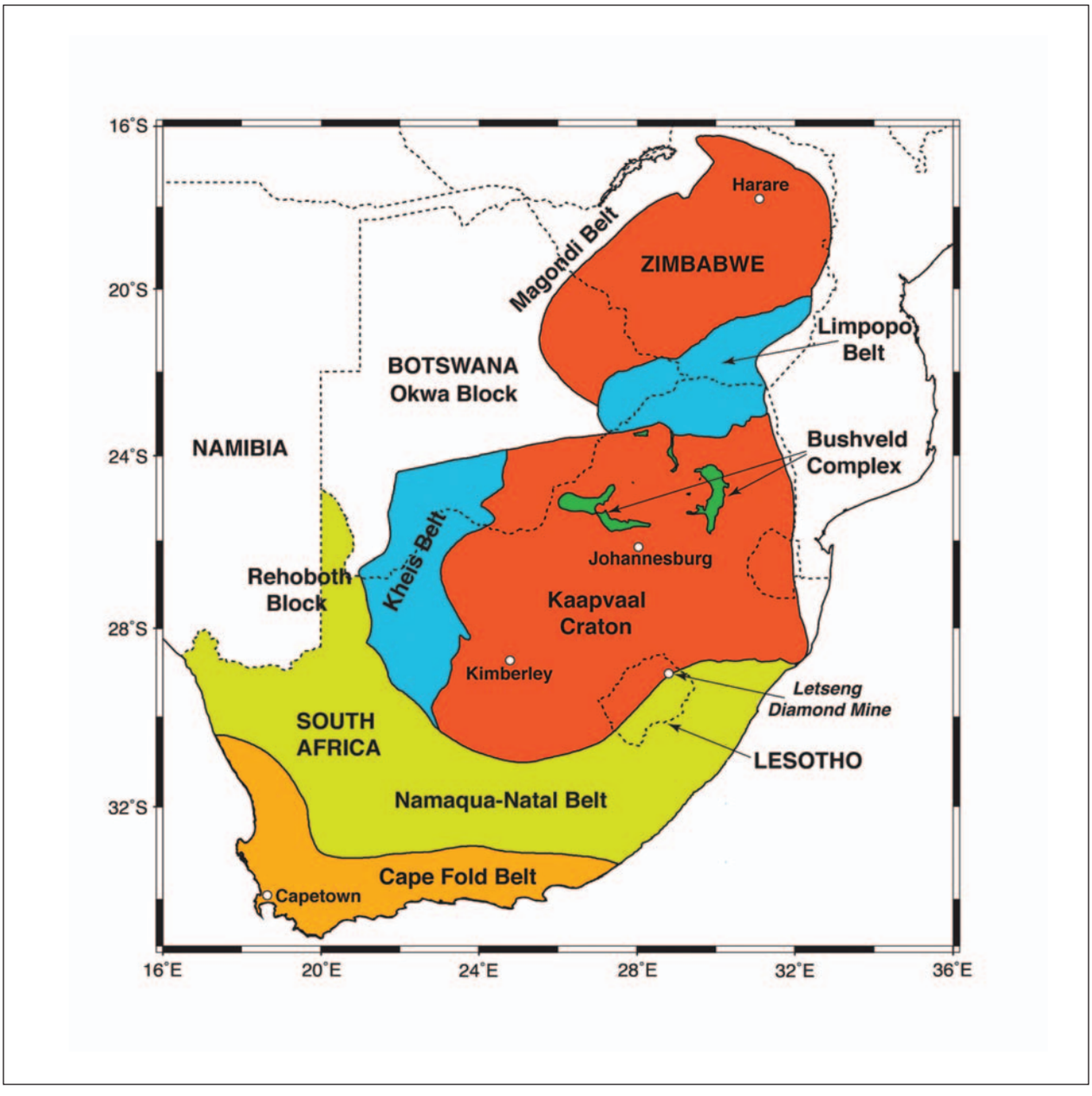

Figure 1. *Overview map showing the principal tectonic domains, terrane boundaries and localities in southern Africa and the location of Letseng-la-Terae Diamond Mine in the eastern part of Lesotho. The map is a modified version and a combination from the studies by Evans et al. (2011) and Niu et al. (2004).*

To produce the regionally extensive low-P and high-T granulites seen in the Namaqua-Natal mobile belt in South Africa, a ~30 km thick mafic underplate would be required, which is a product of interaction between mafic melts and lower crustal rocks. The calculated thickness of the magmatic underplate is based on thermal modelling and is required to produce the peak thermal gradient in the granulite- and upper amphibolite-facies (Waters, 1990). The general difference in crustal thickness between Archaean and Proterozoic crust has been interpreted as a consequence of different mantle lithospheric compositions. Proterozoic crust developed above fertile dense mantle lithosphere, and subsequent partial melting resulted in basaltic underplating and crustal inflation. The ultra-depleted Archaean mantle lithosphere, in contrast, is chemically inert (Durrheim and Mooney, 1994; Lodge et al., 2012; Zartman et al., 2012). These authors also suggested that magmatic underplating explains variations in crustal thickness across the Archaean-Proterozoic boundary between the Kaapvaal craton and the Namaqua-Natal belt. Furthermore, they suggested that mafic granulite xenoliths found in Namaqua-Natal belt kimberlites are derived from the magmatic underplate.

Although zircon age data on meta-igneous and metasedimentary granulite-facies rocks from the lower crust below northeastern Lesotho exist (Schmitz and Bowring., 2004), these data are based on conventional U-Pb dating techniques on abraded zircons and, therefore, core-rim relationships and recrystallization in individual zircon grains were not recorded. For this reason we present single zircon SHRIMP ages and *P-T* calculations for garnet-clinopyroxene-plagioclase bearing intermediate to mafic granulites, supplied by Debbie Bowen of Gemdiamonds in the Letseng-la-Terae Diamond Mine, in order to clarify the age and metamorphic history of these rocks (Figure 1). We address the following questions: 1) was the granulite-facies metamorphic event caused by crustal thickening and/or the injection of hot mantle material, and 2) does the Mesoproterozoic Tugela nappe extend ~200 km farther west as seen in the surface outcrops shown in Figure 2a?

To address these questions we investigated xenolith samples L81582 and L91583. A petrological study has been performed, using EPMA (see appendix) to analyze the mineral chemical composition of the rock-forming minerals in both granulites. The results were subsequently used in geothermobarometric calculations to estimate the *P-T* conditions of granulite-facies metamorphism. A SHRIMP II (see appendix) instrument was used to determine zircon recrystallization ages during granulite-facies metamorphism, and different domains of selected zircon grains were analyzed.

Geological setting and previous geochronology

The Archaean Kaapvaal craton covers an area of ~1.2 million square kilometres and is bound in the north by the late Archaean to Palaeoproterozoic Limpopo Belt (Figure 1). In the south and west the craton is bordered by Proterozoic orogens and to the east by the Lebombo monocline that includes Karoo Jurassic igneous rocks associated with the break-up of Gondwanaland. The Kaapvaal craton was formed and stabilized between ~3.7 and ~2.6 Ga ago and is an amalgamation of Archaean greenstone belts and TTG (tonalite-trondhjemite-granodiorite) gneiss complexes, intruded by different generations of granitoid plutons (Robb et al., 2006).

At its southeastern margin, in KwaZulu-Natal Province, the Kaapvaal craton is bordered by the Tugela terrane (Figure 2a) that is part of the Mesoproterozoic Namaqua-Natal Belt. This belt consists of heterogeneous upper amphibolite- to granulite-facies metasedimentary as well as mafic to intermediate and felsic meta-igneous rocks (Thomas, 1989; Arima and Johnston, 2001; Johnston et al., 2001; Schmitz and Bowring, 2004) and has been divided into three tectonic terranes, which are from north to south Tugela, Mzumbe and Margate.

The Mzumbe and Margate terranes were interpreted as magmatic arcs that formed due to the closure of the Mesoproterozoic Tugela Ocean that was interpreted to have occurred south of the Kaapvaal craton (Figures 3a and b; Matthews, 1972; Matthews and Charlesworth, 1981; Jacobs et al., 1993; Jacobs and Thomas, 1994; Thomas et al., 1994, Johnston et al., 2003). The mafic and ultramafic rocks of the Tugela terrane suggest that they partly represent relicts of oceanic crust (Matthews, 1972).

The Letseng-la-Terae, Matsoku and Mothae kimberlites are located in northeastern Lesotho and form a part of a geographically isolated cluster of about 60 kimberlites that intruded into the volcanic plateau highlands of northeastern Lesotho (Figure 2a). All kimberlite pipes are typically classified as serpentine-monticellite-bearing Group I kimberlites and vary in age between 89 ± 1.4 Ma (Kao; Hoese, 2009), 94.7 ± 1.1 Ma (Matsuko; Hoese, 2009) and 91 ± 2 (Letseng la Terae, Hoese, 2009). Crustal xenoliths are common in the kimberlites and show a large variation in mineral and chemical composition. Garnet-kyanite±orthopyroxene and garnet-clinopyroxene-bearing intermediate granulites, garnet-kyanite±clinopyroxene-bearing felsic granulites, garnet-biotite-bearing granitic gneisses and garnet-biotite-sillimanite-bearing granulite-facies metapelites were found in some of the kimberlites (Schmitz and Bowring, 2004).

Because most of Lesotho is covered by Karoo volcanic plateau highlands, the closest crystalline basement outcrop next to the Letseng-la-Terae mine is located some 200 km to the east, where Mesoproterozoic rocks of the Natal belt have overthrust the southeastern edge of the Kaapvaal craton along the Tugela Front (Schmitz and Bowring, 2004; Figures 2a and b). It has been suggested that the Tugela, Mzumbe and Margate terranes extend much farther to the west below the Karoo volcanic plateau highlands in Lesotho (Schmitz and Bowring, 2004).

The Natal belt is interpreted to have formed through the closure of the Tugela Ocean and accretion of an intra-oceanic arc, the so-called Natal Oceanic Arc, with the Kaapvaal continental margin (Figure 3a), remnants of which are the Mzumbe and Margate terranes consisting of voluminous ~1.2 to ~1.0 Ga granulite-facies rocks and isotopically juvenile granitoids (Thomas, 1989; Thomas et al., 1993; 1999). Ocean basin closure apparently resulted in subcretion of Kaapvaal lithospheric mantle beneath the Natal Oceanic Arc (Figure 2b; Jacob and Thomas, 1994).

The heterogeneous Tugela terrane is poorly understood but can be subdivided into four thrust sheets, which are from east to the west the Nkomo, Madidima, Mandleni and Tugela nappes, respectively (Figure 3b). These thrust sheets consist predominantly of amphibolite-facies gneisses, some showing relict pillow structures, and the entire package was interpreted as a dismembered supra-subduction zone ophiolite sequence that was obducted onto the Kaapvaal craton during the Namaqua-Natal orogeny (Matthews, 1972; 1981; Arima et al., 2001; Johnston et al., 2001; 2003; Figures 3a and b). Thrust faulting and high-grade metamorphism occurred during collision of the oceanic arc and the

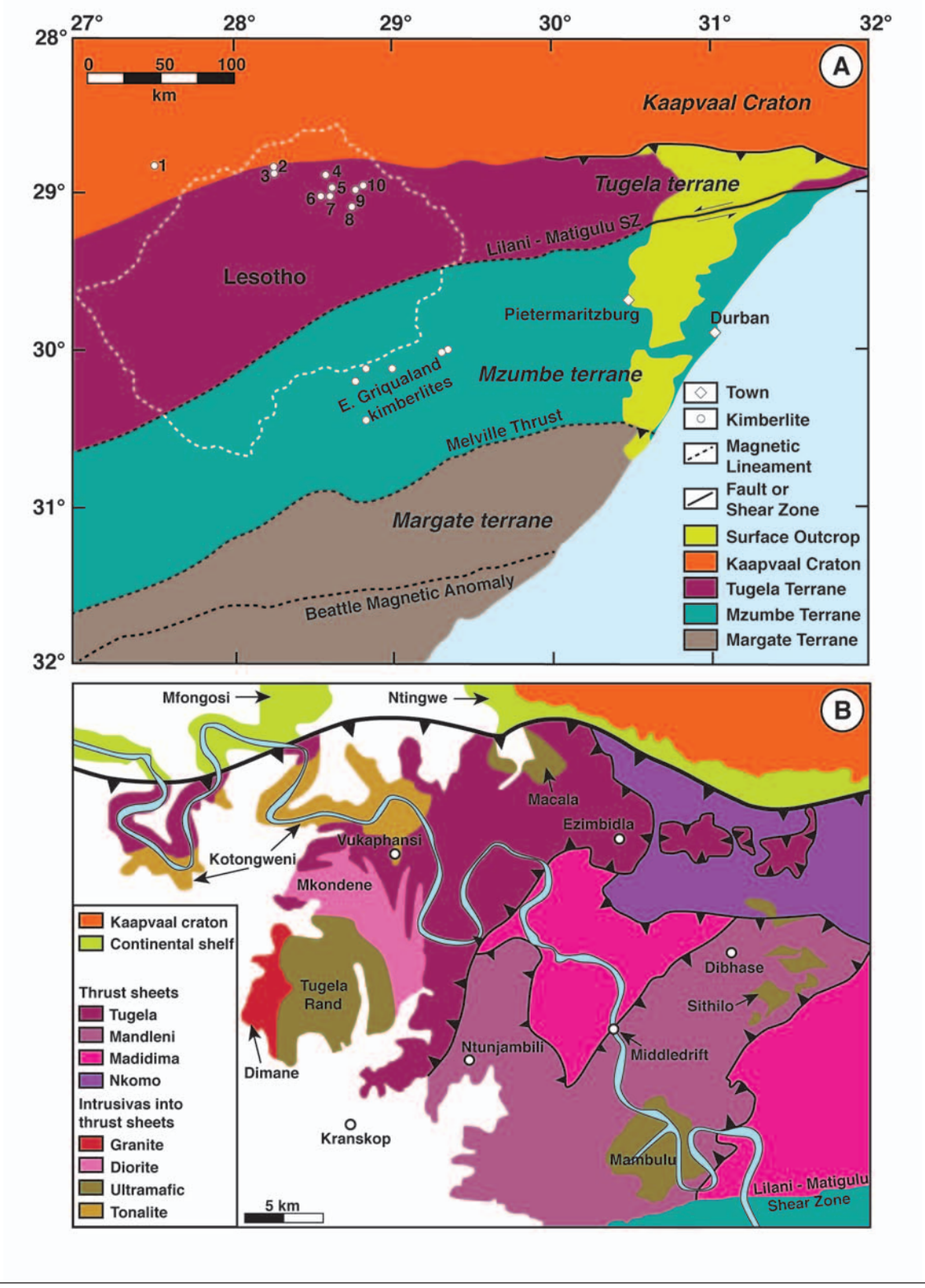

Figure 2. *(**A**) Overview map showing different geological domains around Lesotho and some kimberlite locations (modified after Griffin et al., 1979; Schmitz and Bowring, 2004). From North to South: Kaapvaal craton, Tugela terrane, Mzumbe terrane and Margate terrane. (1) Monastery Mine; (2) Lipelenang; (3) Khabos; (4) Lemphane; (5) Lighobong; (6) Kao; (7) Pipe 200; (8) Matsoku; (9) Mothae; (10) Letseng-la-Terae. (**B**) Figure shows the four thrust sheets and the igneous rocks of the Tugela terrane (modified after Johnston et al., 2003).*

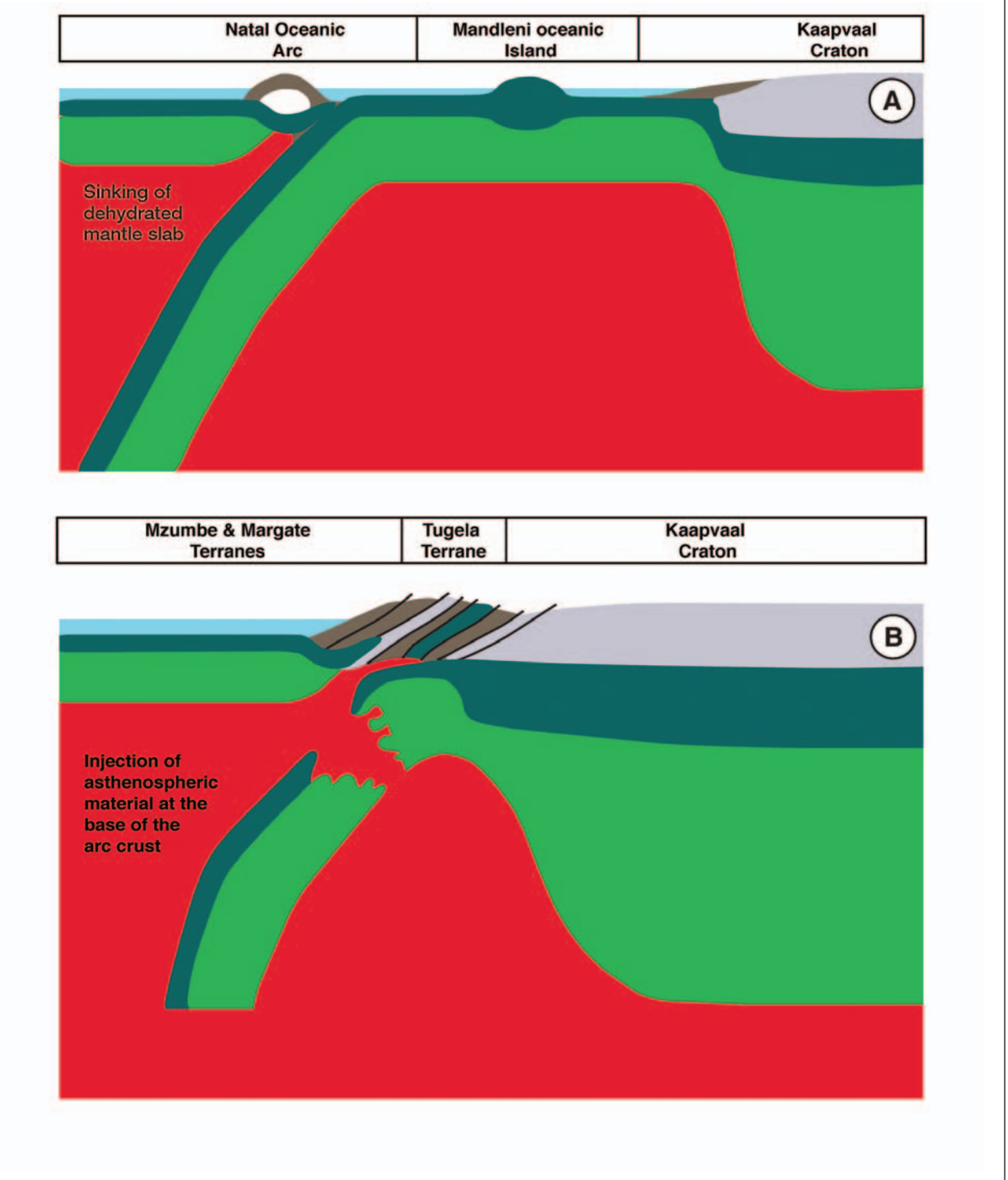

Figure 3. *(**A**) Sketch map showing subduction of the passive margin at the Kaapvaal craton beneath the "Natal Oceanic Arc". Between the "Natal Oceanic Arc" and the "Mandleni Ocaenic Island" was the Tugela Ocean before formation of the Tugela terrain took place (modified after Arima and Johnston, 2003). (**B**) Illustration shows the situation after closure of the Tugela Ocean and the formation of the Tugela- and to the south the Mzumbe and Margate terrains, respectively. Injection of hot asthenosphere into the base of the arc crust is expected after slab roll back and finally break off (modified after Arima and Johnston, 2003).*

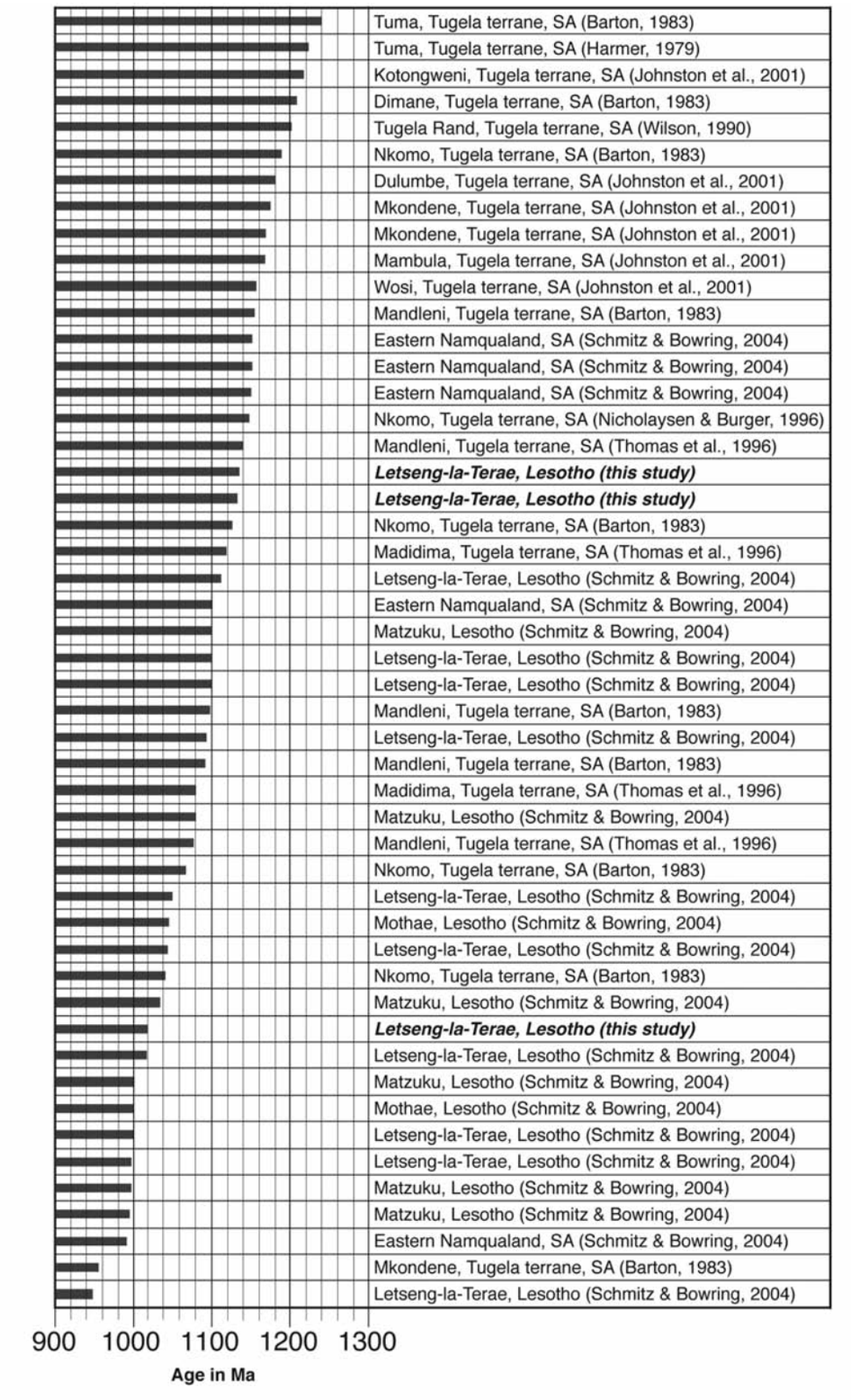

Figure 4. *Age distribution and corresponding locations in the investigated area.*

Table 1. Previous geochronology

Location and rock type	Dating method	Age (Ma)	Interpretation	Reference
Nkomo, Halambu Gneiss	Rb-Sr	780 ± 672	Formation of gneiss metamorphic event	Barton, 1983
Northern Lesotho, Letseng mafic metaigneous granulite	U-Pb (zircon)	948 ± 4	Metamorphic zircon crystallisation	Schmitz & Bowring, 2004
Tugela, Mkondene Diorite (deformed)	Rb-Sr	955 ± 53	Formation of a gneissic zone within the pluton	Barton, 1983
Eastern Namaqualand Klipfontein, garnet granulite	U-Pb (zircon)	991 ± 6	High-grade metamorphism	Schmitz & Bowring, 2004
Northern Lesotho, Matsuko Granitic gneiss	U-Pb (zircon)	~995 to ~997	Metamorphic zircon overgrowth	Schmitz & Bowring, 2004
Northern Lesotho, Letseng felsic metaigneous granulite	U-Pb (zircon)	997 ± 6	Metamorphic zircon crystallisation	Schmitz & Bowring, 2004
Northern Lesotho, Letseng metasedimentary granulite	U-Pb (zircon)	~1000	Metamorphic zircon crystallisation	Schmitz & Bowring, 2004
Northern Lesotho, Mothae metasedimentary granulite	U-Pb (monazite)	1001 ± 2	Younger unzoned growth around older monazite	Schmitz & Bowring, 2004
Northern Lesotho, Matsuko Granitic gneiss	U-Pb (zircon)	~1000	Minimum crystallization age of zircon	Schmitz & Bowring, 2004
Northern Lesotho, Letseng metasedimentary granulite	U-Pb (zircon	~1017	Metamorphic zircon crystallisation	Schmitz & Bowring, 2004
Northern Lesotho, Matsuko mafic metaigneous granulite	U-Pb (zircon)	~1034	Metamorphic zircon crystallisation	Schmitz & Bowring, 2004
Nkomo, Ngoye granite	U-Pb (zircon)	~1041	Emplacement age of magmatic precursor	Barton, 1983
Northern Lesotho, Letseng metasedimentary granulite	U-Pb (monazite)	1044 ± 1	Metamorphic monazite crystallisation	Schmitz & Bowring, 2004
Northern Lesotho, Mothae metasedimentary granulite	U-Pb (monazite)	1045 ± 2	Minimum crystallization age of monazite	Schmitz & Bowring, 2004
Northern Lesotho, Letseng metasedimentary granulite	U-Pb (zircon)	1050 ± 5	Crystallisation of meta-morphic zircon overgrowth	Schmitz & Bowring, 2004
Nkomo, Ngoye granite	Rb-Sr	1067 ± 20	Emplacement of magmatic precursor	Barton, 1983
Mandleni, Dondwana amphibolite	Ar-Ar	1077 ± 11	Amphibolite-facies metamorphism	Thomas et al., 1996
Northern Lesotho, Matsuko Granitic gneiss	U-Pb (zircon)	~1080	Minimum crystallization age of zircon	Schmitz & Bowring, 2004
Madidima, Gazeni amphibolite	Ar-Ar	1080 ± 6	Amphibolite-facies metamorphism	Thomas et al., 1996
Mandleni, Dondwana feldspathic Gneiss	U-Pb (titanite)	~ 1080	Metamorphic cooling age	Barton, 1983
Northern Lesotho, Letseng mafic metaigneous granulite	U-Pb (zircon)	1092 ± 2	Metamorphic zircon crystallisation	Schmitz & Bowring, 2004
Mandleni, Dondwana feldspathic Gneiss	Rb-Sr	1093 ± 108	Referred to as Dondwana Formation	Barton, 1983
Northern Lesotho, Letseng metasedimentary granulite	U-Pb (monazite)	1098 ± 3	Metamorphic monazite crystallisation	Schmitz & Bowring, 2004
Northern Lesotho, Letseng mafic metaigneous granulite	U-Pb (zircon)	~ 1099	Metamorphic zircon crystallisation	Schmitz & Bowring, 2004
Northern Lesotho, Matsuko mafic metaigneous granulite	U-Pb (zircon)	~ 1099	Metamorphic zircon crystallisation	Schmitz & Bowring, 2004
Eastern Namaqualand Witberg, two pyroxene granulite	U-Pb (zircon)	1100 ± 3	High-grade metamorphism	Schmitz & Bowring, 2004
Northern Lesotho, Letseng metasedimentary granulite	U-Pb (monazite)	1104 ± 3	Metamorphic monazite crystallisation	Schmitz & Bowring, 2004
Madidima, Gazeni amphibolite	Ar-Ar	1112 ± 6	Amphibolite-facies metamorphism	Thomas et al., 1996
Nkomo, Halumbu Gneiss	U-Pb (zircon)	~ 1119	Formation of metamorphic event	Barton, 1983
Mandleni, Dondwana amphibolite	Ar-Ar	1135 ± 9	Amphibolite-facies metamorphism	Thomas et al., 1996
Nkomo, Bull's Run Syenite	U-Pb (zircon)	1140 ± 35	Emplacement age of magmatic precursor	Nicolaysen & Burger, 1996
Eastern Namaqualand Markt, garnet biotite gneiss	U-Pb (monazite)	1148 ± 3	Emplacement age of magmatic precursor	Schmitz & Bowring, 2004
Eastern Namaqualand Markt, garnet biotite gneiss	U-Pb (zircon)	1150 ± 5	Emplacement age of magmatic precursor	Schmitz & Bowring, 2004
Eastern Namaqualand Markt, garnet biotite gneiss	U-Pb (monazite)	1152 ± 5	Emplacement age of magmatic precursor	Schmitz & Bowring, 2004
Mandleni, Dondwana feldspathic Gneiss	U-Pb (zircon)	~1152	Referred as Dondwana Formation	Barton, 1983
Tugela, Wosi Granitoid suite	U-Pb (SHRIMP)	1155 ± 1	Emplacement age of magmatic precursor	Johnston et al., 2001
Tugela, Mambula Complex anorthosites	U-Pb (SHRIMP)	~1157	Emplacement age of the Magmatic precursor	Johnston et al., 2001
Tugela, Mkondene Diorite	U-Pb (SHRIMP)	~ 1168	Emplacement age of the magmatic precursor	Johnston et al., 2001
Tugela, Mkondene Diorite	Rb-Sr	1169 ± 142	Emplacement age oft the magmatic precursor	Barton, 1983
Tugela, Dulumbe Paragneiss	U-Pb (SHRIMP)	1175 ± 9	Detrital zircons reflecting age of reworking and deposition	Johnston et al., 2001
Nkomo, Khomo formation	Rb-Sr	1181 ± 126	Referred as Khomo Formation	Barton, 1983
Tugela Rand, layered intrusion	Sm-Nd	1189 ± 14	Emplacement age of the magmatic precursor	Wilson, 1990
Tugela, Dimane Granite	Rb-Sr	1202 ± 84	Emplacement age of the magmatic precursor	Barton, 1983
Tugela, Kotongweni Tonalite Gneiss	U-Pb (SHRIMP)	1209 ± 5	Age of the oceanic Magmatic arc	Johnston et al., 2001
Tugela, Tuma Formation	Rb-Sr	1218 ± 96	Referred as Tuma Formation	Harmer, 1979
Tugela, Tuma Formation	Rb-Sr	1224 ± 88	Referred as Tuma Formation	Barton, 1983
Tugela, Dulumbe Paragneiss	U-Pb (SHRIMP)	1240 ± 10	Detrital zircons reflecting age of reworking and deposition	Johnston et al., 2001
Tugela, Dulumbe Paragneiss	U-Pb (SHRIMP)	1276 ± 10	Detrital zircons reflecting age of reworking and deposition	Johnston et al., 2001
Eastern Namaqualand Klipfontein, garnet granulite	U-Pb (zircon)	1859 ± 7	Emplacement age of the magmatic precursor	Schmitz & Bowring, 2004
Northern Lesotho, Letseng metasedimentary granulite	U-Pb (zircon)	2636 ± 70	Protolith age of the igneous detrital zircon	Schmitz & Bowring, 2004

oceanic plateau terranes with the continental margin of the Kaapvaal craton to the north (Figures 2b and 3b). Ultramafic schists occur along the thrust sheet boundaries and were interpreted as dismembered ophiolites. The strongly deformed Mfongosi and Ntingwe units occur along the northern boundary of the Tugela terrane and are interpreted as continental shelf deposits that formed on the passive margin of the Kaapvaal craton and became tectonically interleaved in the accretionary complex during Grenville-age continent-arc collision (Figure 2b; Jacobs and Thomas, 1994, 1996; Thomas et al., 1999; Arima and Johnston, 2001).

Oceanic magmatism was dated at 1209 ± 5 Ma using zircons. The emplacement age of the magmatic precursors of both the Natal Arc and the in the Tugela Terrane has been constrained at ~1.2 Ga (Barton, 1983; Johnston et al., 2001; Schmitz and Bowring, 2004; Figures 3a and 4; Table 1), based on Rb-Sr and Sm-Nd whole-rock isochrons as well as conventional and SHRIMP (see appendix) zircon and monazite dating. The timing of metamorphism in the Namaqua-Natal belt was constrained between 1104 ± 3 Ma and 948 ± 4 Ma using conventional U-Pb methods on abraded metamorphic zircons and monazites from lower crustal granulite xenoliths from Klipfontein, Witberg, Markt, Mothae, Letseng-la-Terae and Matsoku kimberlites (Schmitz and Bowring, 2004; Figure 4; Table 1), which are all situated on or close to the craton boundary. Amphibolite-facies metamorphism within the Tugela terrane occurred in the Mandleni and Madidima areas, and Ar-Ar ages range between 1080 ± 6 Ma and 1135 ± 9 Ma (Thomas et al., 1996; Table 1, Figures 2b and 4). Ages of detrital zircons vary between 1175 ± 9 Ma and 2636 ± 70 Ma (Johnston et al., 2001; Schmitz and Bowring, 2004; Figure 4; Table 1).

Petrography and petrology

The studied xenolith nodules are intermediate granulites, and the modal mineralogical composition of the rock-forming minerals during peak metamorphic conditions in sample L91583 were garnet (~7%), clinopyroxene (~5%), plagioclase (~71%), and quartz (~12%). Clinopyroxene is partly surrounded by retrograde amphibole (~2%). Biotite (~1%) occurs as small flakes and formed during retrogression after the breakdown of K-feldspar. Accessory minerals are magnetite, rutile, apatite and zircon (~2%). Sample L91583 is a massive rock and does not show any foliation and deformation. Typical grain size varies between 1 and 3 mm. The garnets are homogenous in chemical composition and do not show zonation from core to rim. The analyzed grains show an X_{Alm} ratio between 0.59 and 0.63, X_{Prp} varies between 0.13 and 0.16, and X_{Grs} ranges between 0.20 and 0.26, whereas X_{Spss} is relatively low and shows maximum values of up to 0.01 (Table 2). Clinopyroxene in sample L91583 is diopside according to the classification of Morimoto et al. (1988). X_{Mg} (Mg/Mg + Fe) varies between 0.59 and 0.61, Al_2O_3 is about 2.2 weight %, TiO_2 is about 0.21 weight % and Cr_2O_3 is very low and around 0.04 weight % (Table 2).

Sample L81582 is also an intermediate granulite, but is slightly deformed. Garnets from this sample show lower X_{Alm} and X_{Grs}, higher X_{Pyp} and X_{Sps} ratios compared to those of sample L91583. X_{Alm} varies between 0.45 and 0.48, X_{Pyp} is between 0.31 and 0.35, X_{Grs} ranges between 0.17 and 0.20 and X_{Spss} is up to 0.02 (Table 2). Clinopyroxene in sample L81582 is mostly replaced by wollastonite, which formed during retrogression. Accessory minerals are magnetite, apatite and zircon. The analyzed plagioclase shows nearly the same mineral chemical composition in both samples with a X_{An} ratio ranging between 0.29 and 0.34 (Table 2).

Geothermobarometric calculations has been made in order to estimate the *P-T* conditions during high-grade metamorphism and could only be performed from the mineral pairs in sample L91583 due to the occurrence of clinopyroxene. Only minerals texturally in equilibrium were considered for the *P-T* calculations. To avoid any effect due to retrogression, only mineral core compositions were used to calculate peak metamorphic conditions. We used ion-exchange and net transfer thermometers and barometers and the internally consistent thermodynamic data sets of Berman (1988) for these calculations. The following geothermo-barometers (Ellis and Green, 1979; Moecher et al., 1988; Koziol and Newton, 1989; Berman, 1990) were used for *P-T* calculations of clinopyroxene-bearing mafic to intermediate granulites:

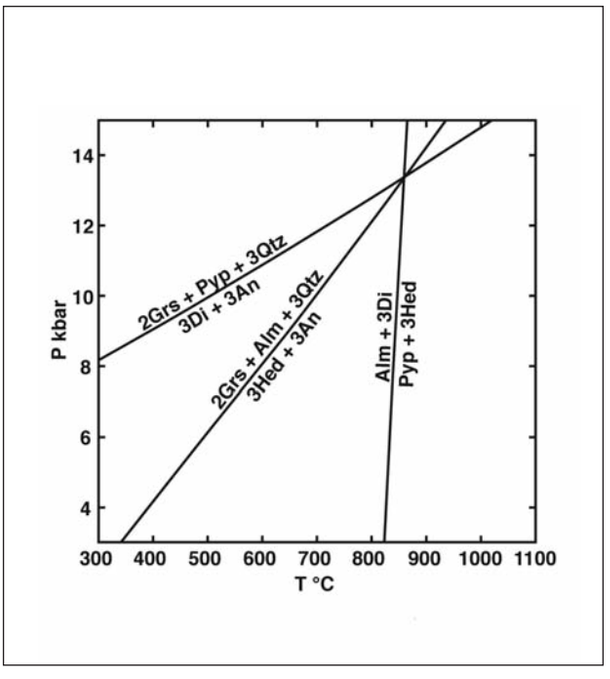

Figure 5. *Temperature and pressure estimates of representative calculations using garnet – clinopyroxene for thermometry and garnet – clinopyroxene – quartz – plagioclase for barometry in granulites from the Letseng-la-Terae Diamond Mine.*

Table 2. Representative EMPA analyses of garnet, clinopyroxene and plagioclase.

Ideal Cations	8.00	8.00	8.00	8.00	4.00	**Ideal Cations**	5.00	5.00	5.00	5.00
Ideal Oxygens	12	12	12	12	6	**Ideal Oxygens**	8	8	8	8
Sample	**L91583 Grt22 Core**	**L91583 Grt51 Core**	**L81582 Grt35 Core**	**L81582 Grt66 Rim**	**L81582 Cpx55 Core**	**Sample**	**L91583 Plag3 Core**	**L91583 Plag6 Core**	**L81582 Plag1 Core**	**L81582 Plag2 Core**
wt %						**wt %**				
SiO_2	38.24	37.26	37.03	37.29	52.36	SiO_2	59.46	60.91	60.37	60.63
TiO_2	0.11	0.06	0.08	0.05	0.21	TiO_2	0.01	0.01	b.d.l	0.01
Al_2O_3	21.43	21.19	22.24	21.49	2.20	Al_2O_3	24.72	24.37	24.17	24.29
Cr_2O_3	0.03	0.02	0.02	0.06	0.04	Cr_2O_3	b.d.l	0.06	0.06	0.05
BaO	b.d.l	b.d.l	b.d.l	b.d.l	b.d.l	BaO	0.17	0.22	0.08	0.06
FeO	28.29	28.24	24.45	24.70	13.13	FeO	0.06	0.05	0.10	0.05
MnO	0.33	0.32	0.89	0.78	0.06	MnO	b.d.l	b.d.l	b.d.l	b.d.l
MgO	4.11	3.16	8.55	7.79	10.60	MgO	b.d.l	b.d.l	b.d.l	b.d.l
CaO	8.00	9.11	5.97	6.26	21.58	CaO	7.24	6.27	6.25	6.13
Na_2O	0.05	0.01	0.04	0.01	0.74	Na_2O	7.74	8.34	8.19	8.29
K_2O	b.d.l	0.01	0.01	b.d.l	b.d.l	K_2O	0.23	0.26	0.64	0.48
Total	100.58	99.38	100.30	98.43	100.92	Total	100.58	100.77	100.92	100.61
Ferric Form	**Grt22**	**Grt51**	**Grt35**	**Grt66**	**Cpx55**	**Ferrous Form**	**Plag3**	**Plag6**	**Plag1**	**Plag2**
Si	2.99	2.96	2.86	2.91	1.97	Si	2.67	2.71	2.70	2.71
Al	1.97	1.98	2.02	1.98	0.10	Al	1.31	1.28	1.28	1.28
Ti	0.01	0.00	0.00	0.00	0.01	Ti	0.00	0.00	0.00	0.00
Cr	0.00	0.00	0.00	0.00	0.00	Cr	0.00	0.00	0.00	0.00
Ba	0.00	0.00	0.00	0.00	0.00	Ba	0.00	0.00	0.00	0.00
Fe_3	0.04	0.09	0.27	0.18	0.01	Mg	0.00	0.00	0.00	0.00
Mg	0.48	0.37	0.98	0.91	0.59	Fe	0.00	0.00	0.00	0.00
Fe	1.81	1.79	1.31	1.43	0.40	Mn	0.00	0.00	0.00	0.00
Mn	0.02	0.02	0.06	0.05	0.00	Ca	0.35	0.30	0.30	0.29
Ca	0.67	0.78	0.49	0.52	0.87	Na	0.67	0.72	0.71	0.72
Na	0.01	0.00	0.01	0.00	0.05	K	0.01	0.01	0.04	0.03
K	0.00	0.00	0.00	0.00	0.00	Sum	5.02	5.02	5.03	5.03
Sum	8.00	8.00	8.00	8.00	4.00					
XPyp/XMg	0.16	0.13	0.35	0.31	0.60	XAn	0.34	0.29	0.30	0.29
XAlm/XFe	0.61	0.60	0.46	0.49	0.40	XAb	0.66	0.71	0.70	0.71
XGrs	0.22	0.26	0.17	0.18	/					
XSps	0.01	0.01	0.02	0.02	/					

almandine + 3diopside = pyrope + 3hedenbergite (1)

almandine + 2grossular = 3quartz + 3hedenbergite + 3anorthite (2)

pyrope + 2grossular = 3quartz + 3diopside + 3anorthite (3)

The measurements used for garnet-clinopyroxene thermometry (1) are based on Fe^{2+} and Mg exchange and persistently yielded temperatures of about 850°C (Figure 5). Pressures were estimated using reactions (2) and (3) above, which provided values around 13 kbar (Figure 5).

Zircon geochronology

Analytical procedures are summarized in the Appendix. Zircons extracted from sample L81582 consist of two varieties, and both groups were dated. One group is characterized by- long-prismatic zircons, ranging in length between 200 and 500 μm, with variable aspect ratios and rounded terminations (Figure 6a). Another group is generally euhedral and often recrystallized or shows newly grown domains that display irregular textures (Figures 6b to e). Most grains are completely recrystallized, and some show metamorphic rims (Figures 6a; b; e). The colour ranges from clear to light grey for zircons from both populations. Fifteen analyses on 11 zircons yielded variably concordant results. Analyses of seven recrystallized zircons and four rims representing metamorphic overgrowth yielded a cluster of data with a weighted mean $^{206}Pb/^{238}U$ age of 1127 ± 6 Ma (MSWD = 0.91; Table 3; Figures 4 and 7). The four metamorphic rims alone yielded a weighted mean $^{206}Pb/^{238}U$ age of 1126 ± 10 Ma (MSWD = 0.51; Table 3; Figures 4 and 7). We interpret both ages to reflect zircon

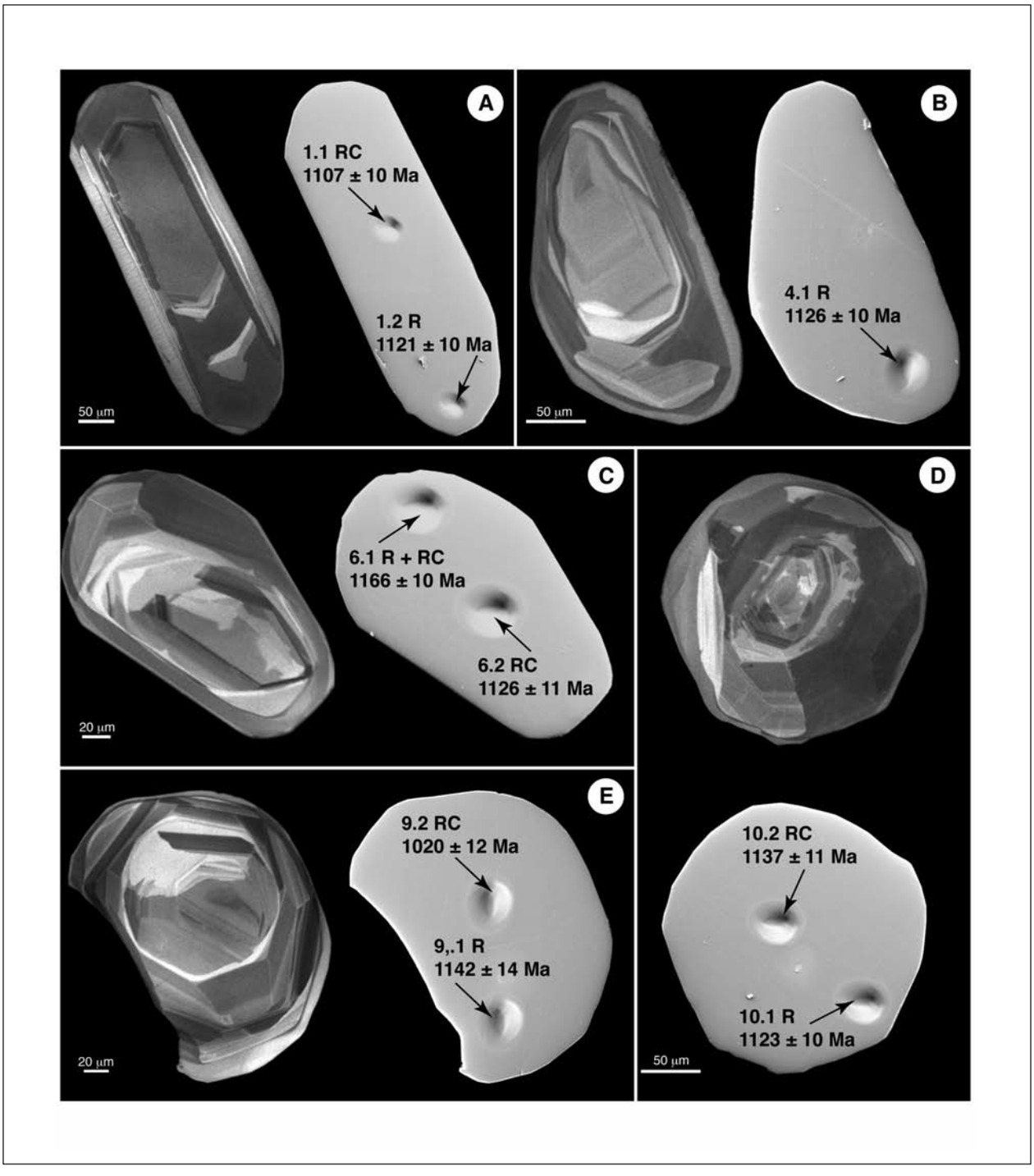

Figure 6. *(**A**) CL image of zircons from granulite (L81582) from Letseng-la-Terae Diamond Mine, showing long-prismatic zircons with rounded terminations and with a recrystallized domain. The positions of the analyzed spots are given by the holes. (**B** to **E**) CL images showing euhedral and often completely recrystallized or newly grown domains that display irregular textures.*

recrystallization and new growth during or close to peak granulite-facies metamorphism.

Zircons extracted from sample L91583 vary in size between 120 and 300 µm, and the grains are also strongly recrystallized and show rounded terminations. Euhedral zircons are often overgrown by recrystallized or newly grown domains that show irregular textures (Figures 8a to d). Eleven spots were analyzed on 10 zircons and yielded a weighted mean $^{206}Pb/^{238}U$ age of 1018 ± 18 Ma (MSWD = 1.5; Table 3; Figures 4 and 9). The large error is due to the very low U and radiogenic Pb contents of the zircons. We also interpret this age to reflect zircon recrystallization and/or overgrowth during granulite-facies metamorphism.

Table 3. SHRIMP U–Pb isotopic data for zircons from granulites from the Letseng-la-Terae Diamond Mine, Lesotho.

Spot	$^{206}Pb_c$ (%)	U (ppm)	Th (ppm)	Th/U	$^{206}Pb^*$ (ppm)	$^{207}Pb^*/^{206}Pb^*$	±%	$^{207}Pb^*/^{235}U$	±%	$^{206}Pb^*/^{238}U$	±%	err corr	$^{206}Pb/^{238}U$ age	$^{207}Pb/^{206}Pb$ age	Discordance (%)
L81582															
1.1RC	0.2	458	90	0.20	73.8	0.0767	0.84	1.980	1.3	0.1873	0.99	0.76	1107 ± 10	1113 ± 17	1
1.2R	0.4	263	42	0.17	43.1	0.0746	1.3	1.954	1.6	0.1899	0.93	0.58	1121 ± 10	1058 ± 27	-6
2.1RC	0.1	257	37	0.15	46.2	0.0807	0.99	2.323	1.4	0.2089	0.99	0.71	1223 ± 11	1213 ± 19	-1
3.1RC	0.1	146	20	0.14	24.4	0.0803	2.0	2.0	2.3	0.1939	1.1	0.49	1143 ± 12	1205 ± 40	5
4.1R	0.2	356	42	0.12	58.6	0.0771	0.94	2.028	1.3	0.1909	0.94	0.70	1126 ± 10	1123 ± 19	0
5.1RC	0.2	398	52	0.14	66.0	0.0749	1.0	1.988	1.4	0.1924	0.90	0.67	1134 ± 9	1067 ± 20	-6
6.1R+RC	0.1	340	44	0.13	57.9	0.0770	0.80	2.105	1.2	0.1982	0.92	0.76	1166 ± 10	1122 ± 16	-4
6.2RC	0.3	192	70	0.38	31.6	0.0764	2.8	2.012	3.0	0.1909	1.1	0.35	1126 ± 11	1106 ± 56	-2
7.1RC	0.4	169	39	0.24	26.5	0.0747	1.7	1.873	2.0	0.1820	1.1	0.53	1078 ± 11	1059 ± 34	-2
8.1RC	0.1	1007	118	0.12	165	0.0771	0.54	2.024	0.99	0.1903	0.83	0.84	1123 ± 9	1125 ± 11	0
9.1R	0.1	396	83	0.22	66.1	0.0781	1.1	2.087	1.7	0.1937	1.4	0.78	1142 ± 14	1150 ± 22	1
9.2RC	0.9	128	33	0.26	19.0	0.0726	5.2	1.715	5.4	0.1715	1.3	0.24	1020 ± 12	1001 ± 110	-2
10.1R	0.2	307	59	0.20	50.3	0.0762	1.1	1.999	1.5	0.1903	0.99	0.66	1123± 10	1100 ± 23	-2
10.2RC	0.3	177	26	0.15	29.4	0.0759	2.6	2.019	2.8	0.1929	1.1	0.39	1137 ± 11	1093 ± 52	-4
11.1RC	0.1	169	78	0.48	29.9	0.0786	1.2	2.229	1.7	0.2058	1.2	0.69	1206 ± 13	1162 ± 24	-4
L91583															
1.1RC	1.35	29	12	0.43	4.60	0.079	9.6	1.97	11	0.1813	5.0	0.47	1074 ± 50	1169 ± 190	8
2.1R	12.85	8	2	0.27	1.24	0.043	89	0.95	90	0.1610	6.2	0.07	965 ± 56	-190 ± 2200	604
2.2RC	6.48	15	5	0.36	2.12	0.065	29	1.38	30	0.1539	5.0	0.17	923 ± 43	776 ± 620	-19
3.1R	3.46	23	7	0.33	3.55	0.069	17	1.69	17	0.1772	3.2	0.19	1052 ± 32	901 ± 350	-17
4.1RC	1.03	83	8	0.10	12.7	0.075	4.8	1.84	5.2	0.1770	2.1	0.40	1050 ± 20	1080 ± 96	3
5.1RC	2.09	39	13	0.34	6.09	0.064	10	1.56	10	0.1761	2.5	0.24	1046 ± 24	754 ± 210	-39
6.1RC	2.39	34	9	0.29	4.96	0.061	14	1.42	14	0.1683	3.7	0.27	1003 ± 35	648 ± 290	-55
7.1RC	1.77	19	7	0.36	2.73	0.099	11	2.25	11	0.1653	2.9	0.26	986 ± 27	1602 ± 200	38
8.1R	2.71	18	4	0.22	2.66	0.079	9.7	1.84	10	0.1687	3.0	0.30	1005 ± 28	1170 ± 190	14
9.1RC	1.89	31	7	0.23	4.54	0.078	13	1.78	13	0.1660	2.7	0.21	990 ± 25	1140 ± 250	13
10.1R	6.17	6	1	0.23	0.9	0.091	52	2.20	52	0.1740	7.0	0.13	1034 ± 67	1448 ± 980	29

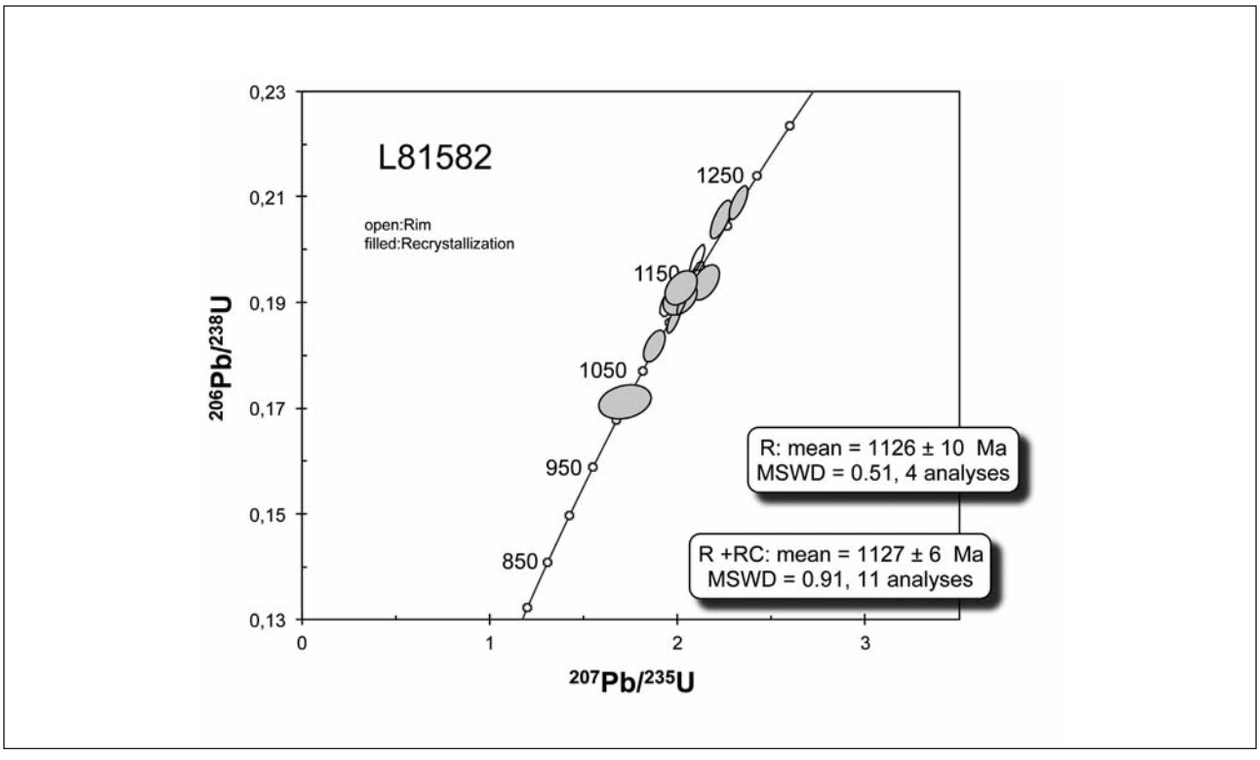

Figure 7. *Concordia diagram showing analytical data for SHRIMP analyses of zircons from granulite sample L81582, Letseng-la-Terae Diamond Mine. Error ellipses for each analysis are defined by standard errors in $^{207}Pb/^{235}U$, $^{206}Pb/^{235}U$ and $^{207}Pb/^{206}Pb$.*

Discussion

The lower crustal granulite xenoliths recovered from kimberlite in the Letseng-la-Terae Diamond Mine contain completely recrystallized zircons, and some grains also exhibit metamorphic rims. Recrystallization and growth of metamorphic rims around zircon occurred between ~1.0 and ~1.1 Ga (Figure 4; Table 1). The peak of granulite-facies metamorphism is reflected by pressures of ~13 kbar and temperatures of ~850°C and is related to a tectono-thermal event interpreted as part of the Namaqua-Natal orogeny (Figure 5). The fact that most analyzed zircons are completely recrystallized supports the idea that the protoliths of the dated samples are older, maybe dating back to the Archaean, and have undergone high-grade metamorphism during the late Mesoproterozoic. This assumption is based on the occurrence of Archaean detrital zircons of igneous origin found in metasedimentary xenoliths recovered from Lesotho kimberlites (Schmitz and Bowring, 2004). The occurrence of different protoliths reflects the compositional variability of the lower crust in northeastern Lesotho, and the ages provide evidence for a thermal overprint at ~1.1 to ~1.0 Ga which corresponds to the timing of events in the Namaqua-Natal belt (Figure 2a). Tectonic interlayering of the juvenile Proterozoic oceanic arc crust with older crustal components during obduction onto the Archaean Kaapvaal craton (Figure 3b) is supported by the variety of the crustal xenoliths found in the Letseng-la-Terae kimberlite.

Based on the age data of two samples, recrystallization and growth of metamorphic rims around zircon appears to have occurred between ~1018 and ~1127 Ma. Thus, high-grade metamorphism and the formation of granulites extended over a considerable period of time and perhaps occurred at different crustal levels. We compare the timing of metamorphic events as shown by the granulite xenoliths at Letseng-la-Terae with granulites exposed ~200 km to the east in the Tugela outcrops. The age of 1127 Ma post-dates the time of obduction of the Tugela terrain onto the Archaean Kaapvaal craton at ~1150 Ma (Jacobs et al., 1997; Arima and Johnston, 2001; Thomas et al., 1996; Barton, 1983). Our age of ~1127 Ma is consistent with amphibolite-facies metamorphism related to crustal thickening along the Archaean cratonic margin that varies between ~1080 and ~1135 Ma (Figure 4, Table 1). Convergence with the Mzumbe terrane in the south was synchronous with obduction of the Tugela terrain (Johnston et al., 2001) and, therefore, provides an additional mechanism for crustal thickening during arc collision.

The age of ~1018 Ma for metamorphic zircons separated from an intermediate granulite xenolith of igneous origin can also be assigned to transtensional deformation as suggested by Schmitz and Bowring (2004). Deformation and metamorphism occurred in the upper part of the lower crust and during likely pre-Grenvillian emplacement of the protoliths. Voluminous granitoid intrusions throughout the Mzumbe and Margate terranes occurred at ~1041 and ~1067 Ma.

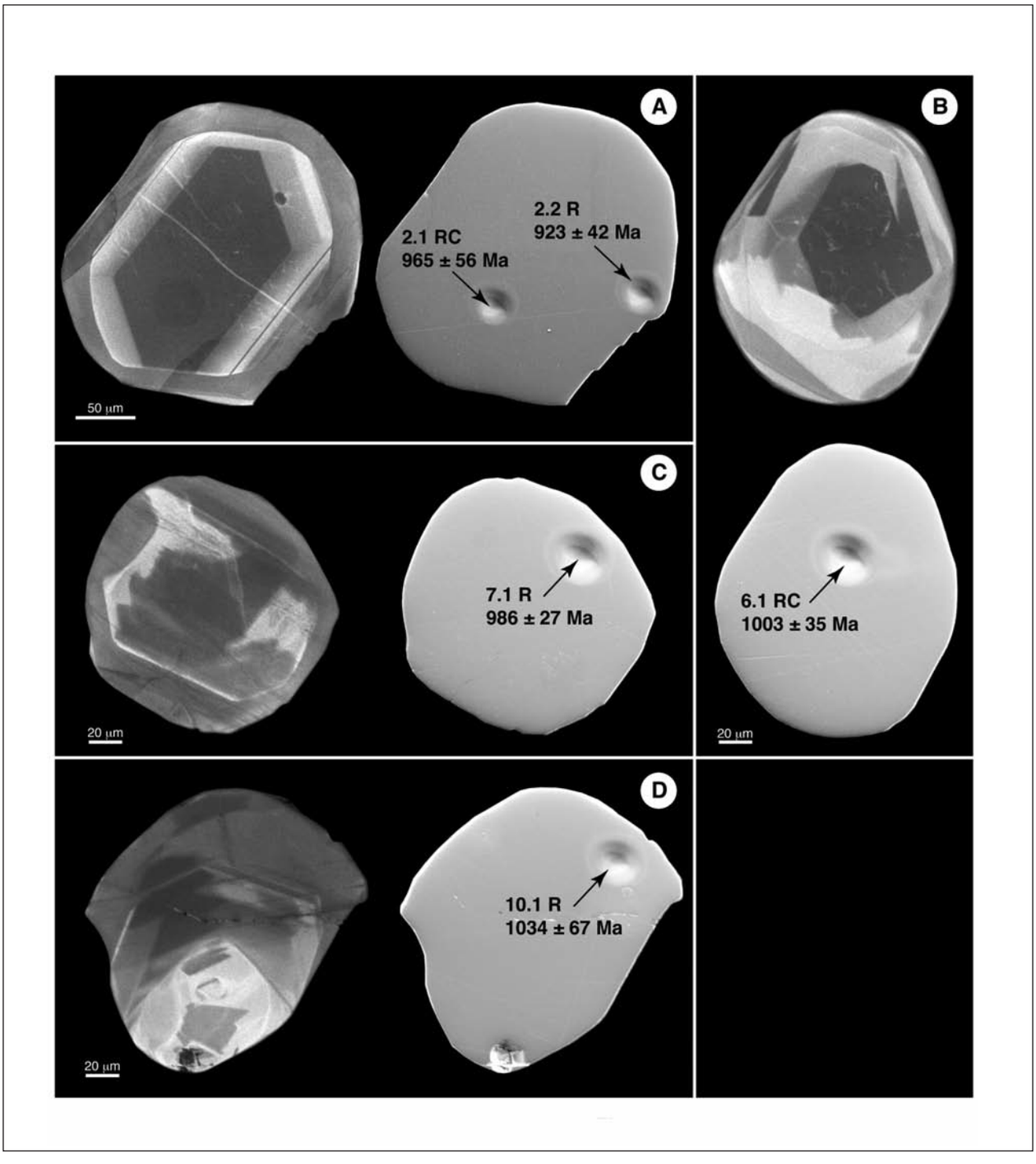

Figure 8. *Images of zircons from granulite sample L91583 from Letseng-la-Terae Diamond Mine, showing strongly recrystallized zircons with rounded terminations. Size varies between 120 and 300 µm. Euhedral zircons are often overgrown by recrystallized or newly grown domains that show irregular textures.*

The age difference of ~100 Ma between the two dated samples reflects the continuous convergence of an accretionary margin over a prolonged period of time. Granulite-facies metamorphism is most likely a result of this continued subduction of arc terranes farther south that generated the Beattie magnetic anomaly (Figure 2a). The abundance of A-type granites emplaced during this event has been used to postulate significant lower crustal melting in the Natal terranes (Thomas et al., 1993) and has also been correlated with emplacement of similar granites formed during *low-P* and *high-T* mid-crustal metamorphism in the western the Namqua Belt (Thomas et al., 1996; Robb et al., 1999). A significant component of advective heat associated with the emplacement of mafic magmas at the base of the crust is necessary to form mid-crustal granulites (Waters, 1990; De Yoreo et al., 1991). Remarkably, no granites ranging in age between ~1.0 and ~1.1 Ga have been found at the

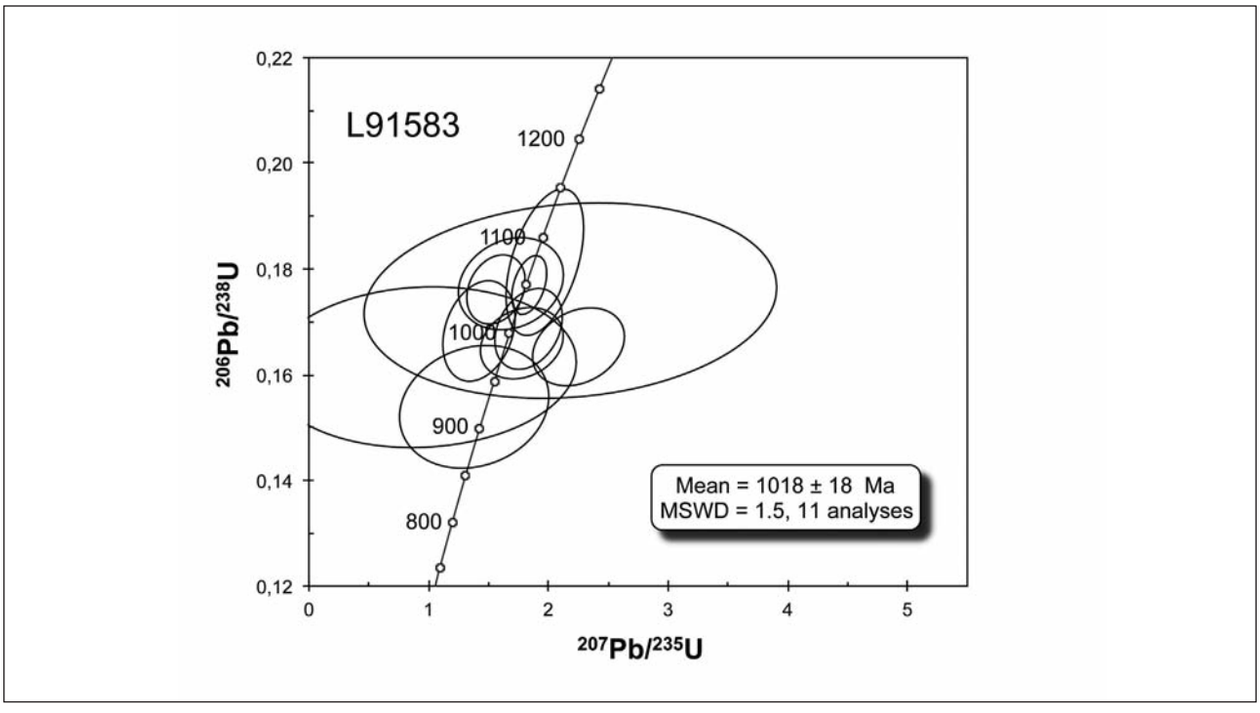

Figure 9. *Concordia diagram showing analytical data for SHRIMP analyses of zircons from granulite sample L91583, Letseng-la-Terae Diamond Mine. Error ellipses as in Figure 7.*

surface in the Tugela terrane nor are there such xenoliths within kimberlites of the Letseng-la-Terae Mine.

Conclusions

Our data provide new evidence for granulite-facies metamorphism to have occurred at ~1127 and ~1018 Ma and at P-T conditions of about 850°C and 13 kbar. The episodic formation of the studied granulites reflects an early event due to collision and crustal thickening and a later event, possibly due to injection of hot asthenosphere into the mantle wedge after assumed slab roll back and eventual slab break-off (Sommer et al., 2012). Such a scenario would cause a change in temperature conditions in the newly formed mantle wedge as a result of slab roll back and slab break off and, therefore, episodic growth and recrystallization of zircon seems possible. Our data suggest that the Tugela nappe extends ca. 200 km farther to the west than previously thought, but this still requires geophysical support.

Acknowledgements

We are grateful to Debbie Bowen of Gem Diamonds for providing the rock samples. We thank the staff of the Beijing SHRIMP Centre for assistance during zircon analysis and data assessment. We are also grateful to Nora Groschopf, Institute of Geosciences, University of Mainz, for assistance during microprobe analyses. We thank Jay Barton for editorial handling of the manuscript and Jelsma Hielke and Jan Kramers for constructive reviews that led to considerable improvement of the manuscript. This is a contribution to IGCP-Project 557.

Appendix

Analytical methods

Six thin sections of two intermediate granulites were investigated by transmitted light microscopy, electron microprobe (EMPA) and a scanning electron microscope (SEM). Mineral analyses were carried out using a JEOL 8900 Superprobe (Mainz University). Standard analytical conditions for silicates were set to an accelerating voltage of 15 kV and 12 nA. Matrix corrections were made using the ZAF procedure. Natural mineral standards were used for calibration. The detection limits in these routine analyses varied from 0.05 to 0.1 weight %. Geothermobarometric calculations were made with the software package TWQ (Bermann, 1992).

Zircon sample preparation

Zircon separation, cathodoluminescence (CL) imaging and U-Pb dating were carried out in the Beijing SHRIMP Centre, Chinese Academy of Geological Sciences. Zircons were separated using routine techniques from approximately 1 to 2 kg of each sample. The grains were mounted in an epoxy discs, polished, and photographed in transmitted and reflected light. CL images of zircons were obtained on a JEOL EPMA with operating conditions at 15 kV accelerating voltage and 12 nA beam current. These images reveal the internal structures in showing high-U (dark) and low-U (bright) domains (Vavra, 1990). However, luminosity is not always correlated with U-content and may also be affected by

REEs (Rubatto and Gebauer, 2000; Stevens Kalceff et al., 2000). Some subtleties in zonation are often visible and are particularly useful for recognizing inherited cores and overgrowth patterns (e.g., Vavra, 1990; Hanchar and Miller, 1993; Vavra et al., 1996).

SHRIMP procedure

The analytical procedures and conditions were similar to those described by Williams (1998). The intensity of the primary $^{2-}$O ion beams was 4 to 6 nA, and spot sizes were ~30 micrometer. Five scans through the mass stations were made for each age determination. Reference standard zircons used were M257 (U = 840 ppm) and TEMORA 1 (^{206}Pb/^{238}U age = 417 Ma) (Black et al., 2003; Nasdala et al., 2008). A common lead correction was applied using the measured ^{204}Pb abundances. Data processing was carried out using the SQUID and ISOPLOT programs (Ludwig, 2001). Uncertainties in the isotopic ratios of individual analyses and on the concordia diagrams are given at 1σ, whereas uncertainties for weighted mean ages in the text and in Figures 6 and 8 are quoted at the 95% confidence level.

References

Arima, M. and Johnston, S.T., 2001. Crustal Evolution of the Tugela Terrane, Natal Belt, South Africa. Gondwana Research, 4, 563-564.

Arima, M., Tani, K., Kawate, S. and Johnston, S.T., 2001. Geochemical characteristics and tectonic setting of metamorphosed rocks in the Tugela terrane, Natal belt, South Africa. Memorial National Institute Polar Research Special Issue, 55, 1-39.

Barton, E.S. (1983). The geochronology of the frontal zones of the Namaqua-Natal Mobile Belt. Unpublished Ph.D. Thesis, University of the Witwatersrand, South Africa, 205pp.

Black, L.P., Kamo, S.L., Allen, C.M., Aleinikoff, J.K., Davis, D.W., Korsch, R.J. and Foudoulis, C., 2003. TEMORA 1: a new zircon standard for Phanerozoic U-Pb geochronology. Chemical Geology, 200, 155-170.

Berman, R. G., 1988. Internally-consistent thermodynamic data for minerals in the system Na_2O-K_2O-CaO-MgO-FeO-Fe_2O_3-AlvO_3-SiO_2-TiOv-HvO-CO_2. Journal of Petrology, 29, 445-522.

Berman, R. G, 1990. Mixing properties of Ca-Mg-Fe-Mn garnets. American Mineralogist, 75, 328-344.

De Yoreo, J.J., Lux, D.R. and Guidotti, C.V., 1991. Thermal modelling in low-pressure/high-temperature metamorphic belts. Tectonophysics, 188, 209-238.

Drummond, B.J. and Collins, C.D.N., 1986. Seismic evidence for underplating of the lower continental crust of Australia. Earth and Planetary Science Letters, 79, 361-372.

Durrheim, R.J. and Mooney, W.D., 1994. Evolution of the Precambrian lithosphere: seismological and geochemical constraints. Journal of Geophysical Research, 99, 15359-15374.

England, P. C. and Thompson, A. B., 1984a. Pressure – Temperature – Time Paths of Regional Metamorphism I. Heat Transfer during the Evolution of Regions of Thickened Continental Crust. Journal of Petrology, 25, 894-928.

England, P.C. and Thompson, A.B., 1984b. Pressure – Temperature – Time Paths of Regional Metamorphism II. Their Inference and Interpretation using Mineral Assemblages in Metamorphic Rocks. Journal of Petrology, 25, 929-955.

Ellis, D. J. and Green, D. H., 1979. An experimental study of the effect of Ca upon garnet-clinopyroxene Fe-Mg exchange equilibria. Contributions to Mineralogy and Petrology, 71, 13-22.

Evans, R.L., Jones, A.G., Garcia, X., Müller, M., Hamilton, M., Evans, S., Fourie, C.J.S., Spratt, J., Webb, S., Jelsma, H. and Hutchins, D., 2011. Electrical lithosphere beneath the Kaapvaal craton, southern Africa. Journal of Geophysical Research, 116, 1-16.

Griffin, W.L., Carswell, D.A. and Nixon, P.H., 1979. Lower crustal granulites and eclogites from Lesotho, South Africa. In: The Mantle Sample: Inclusions in Kimberlites and Other Volcanics. American Geophysical Union, 59-87.

Hanchar, J. M. and Miller, C. F., 1993. Zircon zonation patterns as revealed by cathodoluminescence and backscattered electron images: implications for interpretation of complex crustal histories. Chemical Geology, 110, 1-13.

Hoese, E., 2009. The use of perovskite to explore kimberlite characteristics. Unpublished Honours Thesis, Macquarie University. Australia, 49pp.

Jacobs, J., Falter, M., Thomas, R.J., Kunz, J. and Jessberger, E.K., 1997. ^{40}Ar/^{39}Ar Thermochronological constraints on the structural evolution of the Mesoproterozoic Natal Metamorphic Province, SE Africa. Precambrian Research, 86, 72-91.

Jacobs, J. and Thomas, R. J., 1994. Oblique collision at about 1.1 Ga along the southern margin of the Kaapvaal continent, south-east Africa. Geologische Rundschau, 83, 322-332.

Jacobs, J. and Thomas, R.J., 1996. Pan-African rejuvenation of the c. 1.1 Ga Natal Metamorphic Province (South Africa): K-Ar muscovite and titanite fission track evidence. Journal of the Geological Society, London, 153, 971-978.

Jacobs, J., Thomas, R.J. and Weber., K., 1993. Accretion and indentation tectonics at the southern edge of the Kaapvaal craton during the Kibaran (Grenville) orogeny. Geology, 21, 203-206.

Johnston, S. T., Armstrong, R., Heaman, L., McCourt, S., Mitchell, A., Bisnath, A. and Arima, M., 2001. Preliminary U-Pb Geochronology of the Tugela Terrane, Natal Belt, eastern South Africa. Memorial National Institute Polar Research Special Issue, 55, 40-58.

Johnston, S.T., McCourt, S., Bisnath, A. and Mitchell, A.A., 2003. The Tugela Terrane, Natal belt: Kibaran magmatism and tectonism along the southeast margin of the Kaapvaal Craton. South African Journal of Geology, 106, 85-97.

Koziol, A.M. and Newton, R.C., 1989. Grossular activity-composition relationships in ternary garnets determined by reversed displaced-equilibrium experiments. Contributions to Mineralogy and Petrology, 103, 423-433.

Lodge, A., Nippress, S.E.J., Rietbrock, A., García-Yeguas, A. and Ibáñez., J.M., 2012. Evidence for magmatic underplating and partial melt beneath the Canary Islands derived using teleseismic receiver functions. Physics of the Earth and Planetary Interiors. 212-213, 44-54.

Ludwig, K.R., 2001. Squid 1.02: a user's manual. Berkeley Geochronology Centre Special Publication, Berkeley, California, U.S.A., 1-19.

Matthews, P.E., 1972. Possible Precambrian Obduction and Plate Tectonics in Southeastern Africa. Nature, 240, 37-39.

Matthews, P.E. and Charlesworth, E.G., 1981. Northern margin of the Namaqua – Natal mobile belt in Natal, 1:140 000 scale geological map: Durban, South Africa, University of Natal.

Moecher, D.P., Essene, E.J. and Anovitz, L.M., 1988. Calculation and application of clinopyroxene garnet plagioclase quartz geobarometers. Contribution to Mineralogy and Petrology, 100, 92-106.

Nasdala, L., Hofmeister, W., Norberg, N., Mattinson, J.M., Corfu, F., Dor, W., Kamo, S.L., Kennedy, A.K., Kronz, A., Reiners, P.W., Frei, D., Kosler, J., Wan, Y.S., Goze, J., Hoer, T., Kröner, A. and Valley, A.J., 2008. Zircon M257- a Homogeneous Natural Reference Material for the Ion Microprobe U-Pb Analysis of Zircon. Geostandards and Geoanalytical Reseach, 32, 247-265.

Niu, F., Levander, A., Cooper, C.M., Lee, C.T.A., Lenardic, A. and David E. James, D.E., 2004. Seismic constraints on the depth and composition of the mantle keel beneath the Kaapvaal craton. Earth and Planetary Science Letters, 224, 337-346.

Robb, L.J., Brandl, G., Anhaeusser, C.R. and Poujol, M., 2006. Archaean granitoid intrusions in the Kaapvaal craton. In: M.R. Johnson, C.R., Anhaeusser and R. J. Thomas, (Editors), The Geology of South Africa. Geological Society of South Africa/Council of Geoscience, 1-38.

Robb, L.J., Armstrong, R.A. and Waters, D.J., 1999. The History of Granulite-Facies Metamorphism and Crustal Growth from Single Zircon U-Pb Geochronology: Namaqualand, South Africa. Journal of Petrology, 40, 1747-1770.

Rubatto, D. and Gebauer, D., 2000. Use of cathodoluminescence for U-Pb zircon dating by ion microprobe: some examples from the western Alps. In: M. Pagel, V. Barbin, P. Blanc and D. Ohnenstetter (Editors), Cathodoluminescence in Geosciences. Springer-Verlag, Berlin, Germany, 373-400.

Schmitz, M.D. and Bowring, S.A., 2004. Lower crustal granulite formation during Mesoproterozoic Namaqua-Natal collisional orogenesis, southern Africa. South African Journal of Geology, 107, 261-284.

Sommer, H., Regenauer-Lieb, K., Gasharova., B. and Jung., H., 2012. The formation of volcanic centers at the Colorado Plateau as a result of the passage of aqueous fluid through the oceanic lithosphere and the subcontinental mantle: New implications for the planetary water cycle in the western United States. Journal of Geodynamics, 61, 154-171.

Stevens Kalceff, R. M., Phillips, M. R., Moon, A. R. and Kalceff, W., 2000. Cathodoluminescence microcharacterization of silicon dixide polymorphs. In: M. Pagel, V. Barbin, P. Blanc and D. Ohnenstetter (Editors), Cathodoluminescence in Geosciences. Springer-Verlag, Berlin, Germany. 193-224.

Thomas, R.J., 1989. The petrogenesis of the Mzumbe gneiss suite, a tonalite-trondhjemite orthogneiss suite from the southern part of the Natal structural and metamorphic province. South African Journal of Geology, 92, 322-338.

Thomas, R.J., Agenbacht, A.L.D., Cornell, D.H. and Moore, J.M., 1994. The Kibaran of southern Africa: Tectonic evolution and metallogeny. Ore Geology Reviews, 9, 131-160.

Thomas, R.J., Cornell, D.H. and Armstrong, R.A., 1999. Provenance age and metamorphic history of the Quha Formation, Natal Metamorphic Province: a U-Th-Pb zircon SHRIMP study. South African Journal of Geology, 102, 83-88.

Thomas, R.J., Eglington, B.M., Bowring, S.A., Retief, E.A. and Walravend, F., 1993. New isotope data from a neoproterozoic porphyritic garnitoid-charnockite suite from Natal, South Africa. Precambrian Research, 62, 83-101.

Thomas, R.J., Jacobs, J., Falter, M. and Jessberger, A., 1996. K-Ar and Ar-Ar dating of mineral separates from the Natal metamorphic province. Geological Survey of South Africa Annual Technical Report, 52-56.

Vanderhaeghe, O., 2012. The thermal–mechanical evolution of crustal orogenic belts at convergent plate boundaries: A reappraisal of the orogenic cycle. Journal of Geodynamics, 56-57, 124-145

Vanderhaeghe, O. and Duchene, S., 2010. Crustal-scale mass transfer, geotherm and topography at convergent plate boundaries. Terra Nova, 22, 315-322.

Vavra, G., 1990. On the kinematics of zircon growth and its petrogenetic significance: a cathodoluminescence study. Contributions to Mineralogy and Petrology, 106, 90-99.

Vavra, G., Gebauer, D., Schmidt, R. and Compston, W., 1996. Multiple zircon growth and recrystallization during polyphase late Carboniferous to Triassic metamorphism in granulites of the Ivrea Zone (southern Alps): an ion microprobe (SHRIMP) study. Contributions to Mineralogy and Petrology, 122, 337-358.

Waters, D.J., 1990. Thermal history and tectonic setting of the Namaqualand granulites, southern Africa: clues to Proterozoic crustal development. In: D. Vielzeuf, D. and P.H. Vidal, (Editors), Granulites and crustal evolution., Kluwer Academic Publishers, The Netherlands, 243-256.

Williams, I.S., 1998. U-Th-Pb geochronology by ion microprobe. In: M.A. Mckibben W.C. Shanks and W.I. Ridley (Editors), Applications of Microanalytical Techniques to Understanding Mineralizing Processes. Review in Economic Geology, 7, 1-35.

Zartman, R.E., Kempton, P.D., Paces, J.B., Downes, H., Williams, I.S., Dobosi, G. and Futa, K., 2012. Lower-Crustal Xenoliths from Jurassic Kimberlite Diatremes, Upper Michigan (USA): Evidence for Proterozoic Orogenesis and Plume Magmatism in the Lower Crust of the Southern Superior Province. Journal of Petrology, 54, 575-608.

Editorial handling: J.M. Barton Jnr.